

# C<sup>2</sup>: A Capacity-Centric Architecture Towards Future Wireless Networking

Lu Yang, *MIEEE*, Ping Li, Miaomiao Dong, Bo Bai, *SMIEEE*, Dmitry Zaporozhets, Xiang Chen, Wei Han, *MIEEE*, and Baochun Li, *FIEEE*

**Abstract**—The accelerated convergence of digital and real-world lifestyles has imposed unprecedented demands on today’s wireless network architectures, as it is highly desirable for such architectures to support wireless devices everywhere with high capacity and minimal signaling overhead. Conventional architectures, such as cellular architectures, are not able to satisfy these requirements simultaneously, and are thus no longer suitable for the future era. In this paper, we propose a capacity-centric (C<sup>2</sup>) architecture for future wireless networking. It is designed based on the principles of maximizing the number of non-overlapping clusters with the average cluster capacity guaranteed to be higher than a certain threshold, and thus provides a flexible way to balance the capacity requirement against the signaling overhead. Our analytical results reveal that C<sup>2</sup> has superior generality, wherein both the cellular and the fully coordinated architectures can be viewed as its extreme cases. Simulation results show that the average capacity of C<sup>2</sup> is at least three times higher compared to that of the cellular architecture. More importantly, different from the widely adopted conventional wisdom that base-station distributions dominate architecture designs, we find that the C<sup>2</sup> architecture is not over-reliant on base-station distributions, and instead the user-side information plays a vital role and cannot be ignored.

**Index Terms**—B5G/6G networking architectures, capacity-centric (C<sup>2</sup>), clustering, scalability.

## I. INTRODUCTION

With 5G maturing as the global standard for wireless communications, we are not only experiencing an explosive increase of mobile data traffic, but also witnessing the fusion of real and digital worlds [1], [2]. This phenomenon is anticipated to make our lifestyles more intelligent and automated in the coming era. Various types of intelligent services are emerging, such as autonomous vehicles, immersive media, smart homes, remote healthcare, and factory automation. In the first global 6G Wireless Summit, the concept of ubiquitous wireless intelligence was introduced; wireless connectivity as a part of a critical infrastructure will provide services for both human and non-human users everywhere seamlessly through smart devices and applications [3], [4]. Nevertheless, despite all the initiatives emerging around next-generation wireless systems, its fundamental architecture remains largely undefined.

L. Yang, P. Li, M. Dong, B. Bai, X. Chen, and W. Han are with the Theory Lab, Huawei Technologies Co. Ltd., Hong Kong (e-mail: {yanglu87, liping129, dong.miaomiao, baibo8, chenxiang73, harvey.hanwei}@huawei.com). (The corresponding author is B. Bai.)

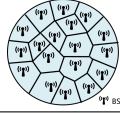
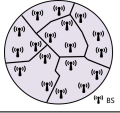
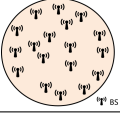
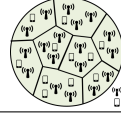
D. Zaporozhets is with the Department of Steklov Mathematical Institute, Russian Academy of Sciences, St. Petersburg, Russia (email: zap1979@gmail.com).

B. Li is with the Department of Electrical and Computer Engineering, University of Toronto, Toronto, Canada (email: bli@ece.toronto.edu).

Cellular networks, which have been commercialized till 5G, are the most classic architectures. A cellular network consists of multiple cells, with each cell corresponding to the coverage area of a base station (BS) [5]. Theoretically, we often use a simplified model of hexagonal cell with a BS in the middle to represent cellular networks [6]. In practice, the locations of deployed BSs are irregular. The coverage map of a cellular network with randomly-located BSs is a Voronoi tessellation [7]–[9], as illustrated in Table I. A cellular architecture is BS-centric, and its main drawback is its poor signal quality at cell edges, where useful signals are affected by heavy interference from other cells. To mitigate the cell-edge problem, an improved architecture called Coordinated Multi-Point transmission (CoMP) was proposed [10]. With CoMP, several closely-located BSs are grouped as a cluster to serve users in a coordinated fashion, illustrated in Table I. A user moving inside a cluster enjoys continuous service, with the cell-edge problem avoided. However, heavy interference still exists at the cluster edges, since CoMP is BS-centric as well. As a result, neither the cellular architecture nor the CoMP architecture is suitable for future wireless systems, given that they cannot guarantee wireless services good enough for users densely located everywhere.

An alternative architecture designed to eliminate the cell-edge problem is a fully coordinated network, where all the BSs are inter-connected for information to be exchanged and optimal decisions to be made [11], [12]. Unfortunately, though such an architecture works in theory, it is not feasible in real-world deployments due to its lack of scalability. In a fully coordinated network, all BSs take part in serving all users with one or several central processing units [13]. The volume of information to be exchanged over fronthaul/backhaul links [14]–[16] expands significantly faster than the increase in the number of network nodes (BSs and users). A substantial amount of signaling overhead and time cost on information delivery, processing, and decision-making will be provoked. This is the reason why the number of inter-connected BSs is always limited in practice. At the late stages of 5G development, a new architecture called cell-free massive MIMO (multiple-input and multiple-output) was proposed and quickly became an active research topic [17]. The basic idea of being “cell free” is to eliminate cell boundaries through interconnecting all the massive MIMO antennas distributed in a geographic area to serve users coherently [18]. There are no cells and thus no cell-edge problems [13], [19]. However, the essence of such an architecture goes back to the design of a fully coordinated network. Although some ideas have been proposed to partially

TABLE I  
COMPARISON OF FOUR WIRELESS NETWORK ARCHITECTURES

Architecture	Cellular	CoMP	Fully Coordinated	Capacity Centric ( $C^2$ )
Toy example of the coverage map				
Design principle	Coverage area of a single BS is a cluster	Several closely-located BSs form a cluster	All BSs participated in serving all users	Average cluster capacity guaranteed and signaling overhead minimized
Architecture type	BS centric			Capacity centric
Architecture robustness	Low The architecture changes with different BS distributions			High
Tessellation	Voronoi Tessellation	BS-centric Tessellation	–	$C^2$ Tessellation ( $C^2T$ )
Relationship with $C^2T$	Extreme case of $C^2T$ ( $M = L$ ) <sup>†</sup>	–	Extreme case of $C^2T$ ( $M = 1$ )	$C^2T$
Scalability	High	Medium	Low	High
Signaling overhead	Low	Medium	High	Low
Capacity	The average cluster capacity per BS can be determined according to Theorem 1.			

<sup>†</sup>  $M$  denotes the number of clusters.  $L$  denotes the number of BSs.

mitigate the lack of scalability [20], such an architecture is still far from being deployed in practice.

In 2017, an idea of decomposing all the BSs and users into non-overlapping clusters was proposed [21]. In this work, the bipartite graph is utilized to model a wireless network, and a network decomposition algorithm was designed based on graph theory. [There are also some follow-up works utilizing the bipartite graphs to model wireless networks and designing network decomposition schemes by graph partition algorithms \[22\], \[23\].](#) However, analytical results on the network decomposition as well as the capacity analysis are still missing. To decompose all the network nodes into non-overlapping clusters is a promising approach for wireless architecture designs. In this paper, we first derive a closed-form expression on the average cluster capacity, by introducing continuous density functions to model the discrete locations of BSs and users in ultra-dense networks. Based on our average cluster capacity theorem, we design a novel capacity-centric ( $C^2$ ) architecture. Different from the conventional BS-centric architectures which only decompose all the BSs into clusters and suffer from the cluster-edge problem, the  $C^2$  architecture can optimally decompose the BSs and users jointly by guaranteeing both high average cluster capacity and superior scalability simultaneously.

The major contributions of this paper are summarized as follows.

- 1) A  $C^2$  architecture for future wireless networking is proposed. It decomposes all the BSs and users into non-overlapping clusters, with the objective of maximizing the number of clusters and guaranteeing the average cluster capacity per BS (or per user) larger than a predefined threshold. On one hand, by guaranteeing the average cluster capacity per BS (or per user) larger than a predefined threshold, all the users can enjoy good-enough wireless services, and the edge problem

in BS-centric architectures is therefore solved in  $C^2$ . On the other hand, by maximizing the number of non-overlapping clusters, the network possesses high scalability with the signaling overhead kept at a minimal level. This is because only BSs belonging to the same cluster are coordinated, and adding or removing network nodes in a cluster will not affect the signaling overhead of other clusters. The unscalability problem in fully coordinated architectures can be solved in  $C^2$  as well. Thus, the  $C^2$  architecture illustrates its potential to improve the overall network performance, while keeps the signaling overhead and computation complexity under control.

- 2) A general and simplified method to determine the capacity is proposed. Specifically, a novel expression of the average cluster capacity per BS (or per user) under the assumption that the numbers of BSs and users approach infinity is derived, as detailed later in Section II-C. This expression is one of the most important foundations of our  $C^2$  architecture, and is widely applicable for wireless systems with different BS and user distributions. Based on this new expression, the capacity region and related performance metrics of an ultra-dense network can be derived with a much lower complexity.
- 3) A comprehensive comparison of different network architectures is presented, and the superiority of our  $C^2$  architecture is shown through performance evaluation. Table I summarizes the characteristics of four different architectures: cellular, CoMP, fully coordinated and  $C^2$ . Our  $C^2$  architecture design takes the information of both BSs and users into consideration, since the capacity is determined by BSs and users jointly. This is the major difference between  $C^2$  and conventional BS-centric architectures (cellular and CoMP), since the latter is designed to focus on the BS-side information

only. In Section III, the generality of the  $C^2$  architecture is presented. Specifically,  $C^2$  can cover almost all the network configurations, wherein the cellular and the fully coordinated architectures can be regarded as two extreme cases. Our simulation results in Section V show that the  $C^2$  architecture outperforms cellular and CoMP networks, with performance gains of at least 300% and 17%, respectively. More importantly, both our theoretical and simulation results disclose that the user distribution plays a non-negligible role in network design. For this reason, conventional BS-centric designs ignoring the user distribution may no longer suitable for future wireless communication systems.

The following content of the paper is organized as follows. The basics of  $C^2$  architecture designs, including the system model, the problem formulation, and the average capacity theorem are introduced in Section II. Section III elaborates the procedures to determine the  $C^2$  architectures with specific network settings, where we take the setting of a constant user density as an example. Section IV visualizes the  $C^2$  architectures based on theoretical results, and derives the capacity region of  $C^2$ . Simulation results on performance comparison across  $C^2$ , CoMP, and cellular architectures are shown in Section V. Section VI concludes the paper, and some detailed proofs are relegated to appendices.

*Notation:* In this paper, scalars and matrices are represented by lowercase and bold uppercase letters, like  $h$  and  $\mathbf{H}$ , respectively, and the  $(i, j)$ -th entry of  $\mathbf{H}$  is denoted by  $[\mathbf{H}]_{i,j}$ . Bold lowercase letters  $\mathbf{x}$  and  $\mathbf{y}$  denotes the location coordinates of the BSs and the users, respectively. Other bold lowercase letters, like  $\mathbf{h}$ , represents the vectors. Scripts such as  $\mathcal{B}$  denote the sets. Notation  $\mathcal{CN}(\mu, \Gamma)$  refers to a complex normal distribution with mean  $\mu$  and variance  $\Gamma$ . Operators  $(\cdot)^H$ ,  $\det(\cdot)$  and  $\mathbb{E}\{\cdot\}$  represent the Hermitian transpose, determinant and expectation, respectively.

## II. $C^2$ DESIGN PRINCIPLES AND AVERAGE CAPACITY THEOREM

### A. System Model

Consider a wireless communication network that constitutes two kinds of nodes:  $L$  single-antenna BSs (or access points in distributed-antenna systems [24]–[27]) and  $K$  single-antenna users [27], [28]. Denote the set of BSs as  $\mathcal{B} = \{b_1, b_2, \dots, b_L\}$ , and the set of users as  $\mathcal{U} = \{u_1, u_2, \dots, u_K\}$ . Assume there are total  $M$  clusters in this network. For the  $j$ th cluster, we use  $\mathcal{C}_j$  to denote the union set of BSs and users in it. The number of BSs in  $\mathcal{C}_j$  is denoted by  $L_j$ , and the number of users in  $\mathcal{C}_j$  is denoted by  $K_j$ . The network architecture is denoted by  $\mathcal{M} = \{\mathcal{C}_1, \mathcal{C}_2, \dots, \mathcal{C}_M\}$ , where  $\{\mathcal{C}_1, \mathcal{C}_2, \dots, \mathcal{C}_M\}$  forms a partition of  $\mathcal{B} \cup \mathcal{U}$ .

The channel gain between BS  $b_l \in \mathcal{C}_j$  and user  $u_k \in \mathcal{U}$  is  $h_{jlk}$ , which can be calculated according to

$$h_{jlk} = \ell_{jlk} \times g_{jlk}. \quad (1)$$

Here,  $g_{jlk} \sim \mathcal{CN}(0, 1)$  is the small-scale fading.  $\ell_{jlk}$  is the large-scale fading, which describes the signal attenuation

between BS  $b_l$  and user  $u_k$  as a function of the signal propagation distance [29], defined as

$$\ell_{jlk} = \left( \theta d_{jlk}^{-\alpha} \right)^{1/2}, \quad (2)$$

where  $d_{jlk}$  is the Euclidean distance between  $b_l$  and  $u_k$ . Parameters  $\theta$  and  $\alpha$  are constants and can take different values based on different path-loss models. In this paper, we use the general form of  $\ell_{jlk}$  (2) for theoretical analysis, and choose an example path-loss model with specific values of  $\theta$  and  $\alpha$  [29] for simulation in Section IV.

The uplink signal model of cluster  $j$  is given by

$$\mathbf{y}_j = \sum_{u_k \in \mathcal{C}_j} \mathbf{h}_{jk} s_k + \sum_{u_\kappa \in \mathcal{U} \setminus \mathcal{C}_j} \mathbf{h}_{j\kappa} s_\kappa + \mathbf{z}_j, \quad (3)$$

where  $\mathbf{h}_{jk}$  is an  $L_j \times 1$  vector, whose  $l$ -th entry is  $h_{jlk}$ .  $s_k \sim \mathcal{CN}(0, P)$  is the information-bearing signal of the user  $u_k$ , with  $P$  as the transmit power of each user.  $\mathbf{z}_j \sim \mathcal{CN}(\mathbf{0}, N_0 \mathbf{I})$  is the additive white Gaussian noise (AWGN) vector.

The average capacity per BS of cluster  $j$  is [6], [30]

$$C_j = \mathbb{E} \left\{ \frac{1}{L_j} \log \det \left[ \mathbf{I} + P(N_0 \mathbf{I} + P \sum_{u_\kappa \in \mathcal{U} \setminus \mathcal{C}_j} \mathbf{h}_{j\kappa} \mathbf{h}_{j\kappa}^H)^{-1} \mathbf{H}_j \mathbf{H}_j^H \right] \right\}, \quad (4)$$

where  $\mathbf{H}_j$  is the channel gain matrix of cluster  $j$ , with  $[\mathbf{H}_j]_{l,k} = h_{jlk}$ . This expression is equivalent to

$$C_j = \mathbb{E} \left\{ \frac{1}{L_j} \log \det \left( \mathbf{I} + P(N_0 \mathbf{I} + \mathbf{\Sigma}_j)^{-\frac{1}{2}} \mathbf{H}_j \mathbf{H}_j^H (N_0 \mathbf{I} + \mathbf{\Sigma}_j)^{-\frac{1}{2}} \right) \right\}, \quad (5)$$

where  $\mathbf{\Sigma}_j$  denotes the inter-cluster interference, and can be regarded as a diagonal matrix with the  $l$ -th diagonal entry as

$$[\mathbf{\Sigma}_j]_{l,l} = \sum_{u_\kappa \in \mathcal{U} \setminus \mathcal{C}_j} \mathbb{E} \{ |h_{jlk}|^2 \} P = P \sum_{u_\kappa \in \mathcal{U} \setminus \mathcal{C}_j} \ell_{jlk}^2 = P \sum_{u_\kappa \in \mathcal{U} \setminus \mathcal{C}_j} \theta d_{jlk}^{-\alpha}. \quad (6)$$

If we define the equivalent channel gain matrix  $\tilde{\mathbf{H}}_j$  as

$$\tilde{\mathbf{H}}_j = (N_0 \mathbf{I} + \mathbf{\Sigma}_j)^{-\frac{1}{2}} \mathbf{H}_j. \quad (7)$$

The average cluster capacity per BS (5) becomes

$$C_j = \mathbb{E} \left[ \frac{1}{L_j} \log \det \left( \mathbf{I} + P \tilde{\mathbf{H}}_j \tilde{\mathbf{H}}_j^H \right) \right]. \quad (8)$$

To capture the ultra-dense characteristics of future networks, we assume that both  $K$  and  $L$  approach infinity, and the ratio between  $K$  and  $L$  is denoted as  $\beta$ . Similarly, for the cluster  $j$ , we assume both  $K_j$  and  $L_j$  approach infinity with  $\frac{K_j}{L_j} = \beta_j$ . Denote  $C_j^\infty$  as the average cluster capacity per BS under such asymptotic assumptions, and we have

$$C_j^\infty = \lim_{\substack{K_j, L_j \rightarrow \infty \\ K_j / L_j = \beta_j}} C_j = \lim_{\substack{K_j, L_j \rightarrow \infty \\ K_j / L_j = \beta_j}} \mathbb{E} \left[ \frac{1}{L_j} \log \det \left( \mathbf{I} + P \tilde{\mathbf{H}}_j \tilde{\mathbf{H}}_j^H \right) \right]. \quad (9)$$

### B. Design Principles and Problem Formulation

Our objective is to design a network architecture  $\mathcal{M}$ , which not only provides high-quality wireless services everywhere, but also possesses good scalability suitable for real-world deployments. Thus, our design principles of a brand-new

architecture towards future wireless communications include the following two aspects. On one hand, to guarantee high-quality wireless services everywhere, we set the average cluster capacity larger than a predetermined threshold  $C_{Th}$ . This threshold can be designed based on specific requirements in practice. On the other hand, to achieve good scalability, we organize all the network nodes into  $M$  ( $1 \leq M \leq L$ ) disjoint clusters. BSs in the same cluster coordinate to serve the users, but work independently if located in different clusters. As such, information is exchanged inside each cluster. The scale of the induced signaling overhead is restricted by the cluster size. Different from a fully coordinated network, the signaling overhead of the entire network will not fluctuate substantially due to the increase or decrease of a single network node. More specifically, we should maximize the number of clusters  $M$ , since the larger  $M$  corresponds to the smaller cluster size and the less signaling overhead. In what follows, we will present a detailed theoretical study that incorporate these principles for designing our  $C^2$  architecture.

First, the problem of maximizing the number of clusters while satisfying the capacity requirement can be formulated in a concise form as

$$\mathcal{P}1: \max_{\mathcal{M}} M, \quad (10)$$

$$s.t. \quad C_j^\infty \geq C_{Th}, \quad \forall j \in \{1, 2, \dots, M\},$$

Note that  $C_j^\infty$  is the average cluster capacity per BS, and the average cluster capacity per user is  $C_j^\infty/\beta_j$ , which is a scaled version of  $C_j^\infty$ . Thus, the constraint in  $\mathcal{P}1$  guarantees the communication quality of each BS or each user larger than a predefined threshold. Next, to solve  $\mathcal{P}1$ , we start from analyzing  $C_j^\infty$ .

### C. Average Cluster Capacity Theorem

It can be observed from (9) that high-dimensional matrix manipulation should be performed in order to determine  $C_j^\infty$ . This will lead to high difficulty and complexity to solve  $\mathcal{P}1$ . In the following, we will introduce our proposed theorem to determine  $C_j^\infty$  in a much simplified and ingenious way.

*Lemma 1:* If  $K_j, L_j \rightarrow \infty$  with  $\frac{K_j}{L_j} = \beta_j$ ,  $\tilde{\mathbf{H}}_j \tilde{\mathbf{H}}_j^H$  become a diagonal matrix, and its asymptotic behavior is given by

$$\lim_{\substack{K_j, L_j \rightarrow \infty \\ K_j/L_j = \beta_j}} \tilde{\mathbf{H}}_j \tilde{\mathbf{H}}_j^H \xrightarrow{P} \text{diag}(\lambda_{1j}, \lambda_{2j}, \dots, \lambda_{L_j j}), \quad (11)$$

where  $\xrightarrow{P}$  denotes the convergence in probability, and  $\lambda_{lj}$  is given by

$$\lambda_{lj} = \frac{\sum_{u_k \in \mathcal{U}_j} \ell_{jlk}^2}{N_0 + \sum_{u_k \in \mathcal{U} \setminus \mathcal{C}_j} \ell_{jlk}^2 P}, \quad \forall l \in \{1, 2, \dots, L_j\}. \quad (12)$$

*Proof:* Please see Appendix A.  $\blacksquare$

Based on Lemma 1 and the concavity of the log-determinant function, we have

$$C_j^\infty = \lim_{\substack{K_j, L_j \rightarrow \infty \\ K_j/L_j = \beta_j}} \mathbb{E} \left[ \frac{1}{L_j} \log \det \left( \mathbf{I} + P \tilde{\mathbf{H}}_j \tilde{\mathbf{H}}_j^H \right) \right] \quad (13)$$

$$= \lim_{\substack{K_j, L_j \rightarrow \infty \\ K_j/L_j = \beta_j}} \frac{1}{L_j} \sum_{l=1}^{L_j} \log(1 + P \lambda_{lj}).$$

For further analysis, with the asymptotic assumptions, the expression (12) can be transformed by replacing the discrete distributions of the network nodes by continuous density as follows.

Let  $\mathcal{D}_0$  denote the two-dimensional region spanning the entire network, and let  $\mathcal{D}_j \subseteq \mathcal{D}_0$  denote the region spanned by the  $j$ -th cluster. Note that the set  $\{\mathcal{D}_1, \mathcal{D}_2, \dots, \mathcal{D}_M\}$  is a partition of  $\mathcal{D}_0$ . With a slight abuse of notation, we use  $|\mathcal{D}_0|$  to denote the area of  $\mathcal{D}_0$ , and  $|\mathcal{D}_j|$  to denote the area of  $\mathcal{D}_j$ . Assume BSs and users are distributed over  $\mathcal{D}_0$  according to continuous density functions  $\rho_b(\mathbf{x})$  and  $\rho_u(\mathbf{y})$ , with  $\mathbf{x}$  and  $\mathbf{y}$  representing the location coordinates of the BSs and users, respectively. Then  $\lambda_{lj}$  (12) can be represented by a continuous form as

$$\lambda_{lj} = \frac{\int_{\mathbf{y} \in \mathcal{D}_j} f(\mathbf{x} - \mathbf{y}) \rho_u(\mathbf{y}) d\mathbf{y}}{N_0 + P \int_{\mathbf{y} \in \mathcal{D}_0 \setminus \mathcal{D}_j} f(\mathbf{x} - \mathbf{y}) \rho_u(\mathbf{y}) d\mathbf{y}}, \quad (l = 1, 2, \dots, L_j), \quad (14)$$

where

$$f(\mathbf{x} - \mathbf{y}) = \theta d_{\mathbf{xy}}^{-\alpha}, \quad (15)$$

defined as the square of large-scale fading, with  $d_{\mathbf{xy}}$  denoting the Euclidean distance between the BS with coordinates  $\mathbf{x}$  and the user with coordinates  $\mathbf{y}$ . Similarly, by transforming other items in (13) from discrete forms into continuous ones, and based on Cauchy's Mean Value Theorem [31], we derive a new expression to determine  $C_j^\infty$  as follows.

*Theorem 1 (Average cluster capacity):* Conditioning on the number of BSs and the number of users approaching infinity, the average cluster capacity per BS is given by

$$C_j^\infty = \log \frac{\frac{N_0}{P} + \int_{\mathbf{y} \in \mathcal{D}_0} f(\mathbf{x}_{jl} - \mathbf{y}) \rho_u(\mathbf{y}) d\mathbf{y}}{\frac{N_0}{P} + \int_{\mathbf{y} \in \mathcal{D}_0 \setminus \mathcal{D}_j} f(\mathbf{x}_{jl} - \mathbf{y}) \rho_u(\mathbf{y}) d\mathbf{y}}, \quad (16)$$

for some BS  $b_l$  in the  $j$ th cluster with coordinate denoted by  $\mathbf{x}_{jl}$ .

*Proof:* By transforming all the items in (13) from discrete forms into continuous ones, including replacing the discrete distributions of the network nodes by continuous distributions, and replacing the summation by the integral, we have

$$C_j^\infty = \lim_{\substack{K_j, L_j \rightarrow \infty \\ K_j/L_j = \beta_j}} \frac{1}{L_j} \sum_{l=1}^{L_j} \log(1 + P \lambda_{lj})$$

$$= \lim_{\substack{K_j, L_j \rightarrow \infty \\ K_j/L_j = \beta_j}} \frac{1}{L_j} \sum_{l=1}^{L_j} \log \left( \frac{\frac{N_0}{P} + \sum_{u_k \in \mathcal{U}} \ell_{jlk}^2}{\frac{N_0}{P} + \sum_{u_k \in \mathcal{U} \setminus \mathcal{C}_j} \ell_{jlk}^2} \right)$$

$$= \frac{1}{\int_{\mathbf{x} \in \mathcal{D}_j} \rho_b(\mathbf{x}) d\mathbf{x}} \int_{\mathbf{x} \in \mathcal{D}_j} \rho_b(\mathbf{x}) \log \frac{\frac{N_0}{P} + \int_{\mathbf{y} \in \mathcal{D}_0} f(\mathbf{x} - \mathbf{y}) \rho_u(\mathbf{y}) d\mathbf{y}}{\frac{N_0}{P} + \int_{\mathbf{y} \in \mathcal{D}_0 \setminus \mathcal{D}_j} f(\mathbf{x} - \mathbf{y}) \rho_u(\mathbf{y}) d\mathbf{y}} d\mathbf{x}$$

$$= \log \frac{\frac{N_0}{P} + \int_{\mathbf{y} \in \mathcal{D}_0} f(\mathbf{x}_{jl} - \mathbf{y}) \rho_u(\mathbf{y}) d\mathbf{y}}{\frac{N_0}{P} + \int_{\mathbf{y} \in \mathcal{D}_0 \setminus \mathcal{D}_j} f(\mathbf{x}_{jl} - \mathbf{y}) \rho_u(\mathbf{y}) d\mathbf{y}}, \quad (17)$$

for some  $\mathbf{x}_{jl} \in \mathcal{D}_j$ , where the last equation follows Cauchy's Mean Value Theorem [31].  $\blacksquare$

Theorem 1 provides a substantially simplified expression to determine  $C_j^\infty$ , where neither the high-dimensional matrix manipulation nor the eigenvalue derivation is needed. This

expression is sufficiently general to be applied in various networks, since it does not have any constraints on the network node distributions, the network area, and the cluster areas. In addition, Theorem 1 reveals that the user density function  $\rho_u(\mathbf{y})$  plays an important role in determining  $C_j^\infty$ , and thus further affects the network architecture design  $\mathcal{M}$ . Conventional BS-centric architectures have their disadvantages such as cell-edge problems, due to the missing role from the user's side.

### III. THE $C^2$ ARCHITECTURE WITH A CONSTANT USER DENSITY

In this section, we will elaborate how a  $C^2$  architecture is to be derived with a specific network setting. As aforementioned, both the problem formulation  $\mathcal{P}1$  and Theorem 1 are adaptive to different network settings. In the following, we will take the setting of a constant user density as an example case to derive the  $C^2$  architecture.

With a constant user density,  $\rho_u(\mathbf{y})$  can be simplified as  $\rho_u$ , unrelated to user location coordinates  $\mathbf{y}$ . Such a distribution is also known as a Poisson distribution. By substituting  $\rho_u$  for  $\rho_u(\mathbf{y})$  in (16), and focusing on the interference-limited regime where the background noise can be ignored, we can determine the average cluster capacity per BS according to the following corollary.

*Corollary 1 (Average cluster capacity with a constant user density):* Conditioning on a constant user density, and the number of BSs and users approaching infinity, the average cluster capacity per BS is given by

$$C_j^\infty = \log \frac{\int_{\mathbf{y} \in \mathcal{D}_0} f(\mathbf{x}_{jl} - \mathbf{y}) d\mathbf{y}}{\int_{\mathbf{y} \in \mathcal{D}_0 \setminus \mathcal{D}_j} f(\mathbf{x}_{jl} - \mathbf{y}) d\mathbf{y}}, \quad (18)$$

for some BS  $b_l$  in the  $j$ th cluster with coordinates denoted by  $\mathbf{x}_{jl}$ .

Corollary 1 reveals that with a constant user density and a given cluster region,  $C_j^\infty$  is determined by a certain BS location inside this cluster. In addition, it reveals that  $C_j^\infty$  is positively correlated to the cluster area  $|\mathcal{D}_j|$ . As such, the constraints in  $\mathcal{P}1$  can be transformed to the cluster area  $|\mathcal{D}_j|$  larger than a given area threshold  $|\mathcal{D}_{Th}|$ . The problem of maximizing the number of clusters while satisfying the capacity requirement under the condition of a constant user density can be reformulated as

$$\mathcal{P}2: \quad \max_M M, \quad (19)$$

$$\text{s.t.} \quad |\mathcal{D}_j| \geq |\mathcal{D}_{Th}|, \quad \forall j \in \{1, 2, \dots, M\}.$$

Combining the constraint in  $\mathcal{P}2$  and the fact of  $\sum_{j=1}^M |\mathcal{D}_j| = |\mathcal{D}_0|$ , we can obtain the optimal number of clusters  $M^*$  and the optimal cluster area  $|\mathcal{D}_j^*|$  as

$$M^* = \left\lfloor \frac{|\mathcal{D}_0|}{|\mathcal{D}_{Th}|} \right\rfloor, \quad |\mathcal{D}_j^*| = |\mathcal{D}_{Th}|, \quad (20)$$

where  $\lfloor x \rfloor$  is the floor function giving the greatest integer less than or equal to the input value  $x$ . We can conclude that an optimal network architecture keeps the signaling overhead

at a minimal level while guaranteeing good-enough wireless services, and can be designed based on (20).

Let's go a step further to analyze the optimal solutions (20). If we set  $|\mathcal{D}_{Th}|$  to be equal to  $|\mathcal{D}_0|$ , the extreme case  $M^* = 1$  arises, corresponding to a fully coordinated network architecture, with a maximized network capacity but the highest signaling overhead. If  $|\mathcal{D}_{Th}| = |\mathcal{D}_0|/L$ , another extreme case  $M^* = L$  arises, corresponding to the cellular architecture, with the number of clusters equal to the number of BSs. The cluster capacity in this case is the worst, but the signaling overhead of each cluster is the lowest. As such, we can claim that our  $C^2$  architecture is sufficiently general, in which both the cellular and fully coordinated networks can be regarded as extreme cases.

Another important finding is that with a fixed user density, the  $C^2$  architecture can be determined directly according to (20), not over-reliant on the BS distributions. Thus, the user-side information plays a vital role in determining  $C^2$  architectures, and should not be ignored in future wireless architecture designs.

### IV. $C^2$ VISUALIZATION AND CAPACITY REGION ANALYSIS

Based on our derived results in Section III, we now visualize the  $C^2$  architectures and perform the capacity analysis with more explicit network settings, including the path-loss parameters, the shapes of the network region  $\mathcal{D}_0$  and the cluster region  $\mathcal{D}_j$ .

#### A. Visualization of $C^2$ Architectures

Assume both  $\mathcal{D}_0$  and  $\mathcal{D}_j$  are round with radius denoted by  $R_0$  and  $R_j$ , respectively. The centers of  $\mathcal{D}_0$  and  $\mathcal{D}_j$  are denoted as  $O_0$  and  $O_j$ , with coordinates  $\mathbf{x}_{O_0}$  and  $\mathbf{x}_{O_j}$ , respectively. With a constant user density, the optimal number of clusters  $M^*$  and the optimal cluster radius  $R_j^*$  for all  $j \in \{1, 2, \dots, M\}$  can be derived based on (20) as

$$M^* = \left\lfloor \frac{R_0^2}{R_{Th}^2} \right\rfloor, \quad R_j^* = R_{Th}. \quad (21)$$

Note that these results are obtained without constraints on the distribution of BSs.

For visualization, we plot two  $C^2$  architectures in Fig. 1. The case of BSs deployed with a constant density  $\rho_u$  is shown in Fig. 1(a). The case of BSs deployed centrally dense and peripherally sparse is shown in Fig. 1(b). Specifically, to simulate the latter case, we divide the entire round network region  $\mathcal{D}_0$  into three concentric subregions, with radius intervals  $[0, \frac{1}{3}R_0]$ ,  $[\frac{1}{3}R_0, \frac{2}{3}R_0]$ , and  $[\frac{2}{3}R_0, R_0]$ , respectively. With a given  $\rho_u$ ,  $\rho_b$  can be calculated according to  $\rho_b = \rho_u/\beta$ . Then, we choose three different BS densities:  $\frac{5}{9}\rho_b$ ,  $\frac{3}{9}\rho_b$ ,  $\frac{1}{9}\rho_b$ , and allocate them to the three concentric subregions from the innermost to the outermost sequentially. Such a setting is to emulate real-world scenarios with a larger number of BSs in the central urban area, and fewer BSs in the surrounding rural area. It can be observed from Fig. 1 that both  $M^*$  and  $R_j^*$  are the same for the above two cases. It implies that the  $C^2$  architecture is unrelated to the BS distributions, as long as the users are distributed with a constant density.

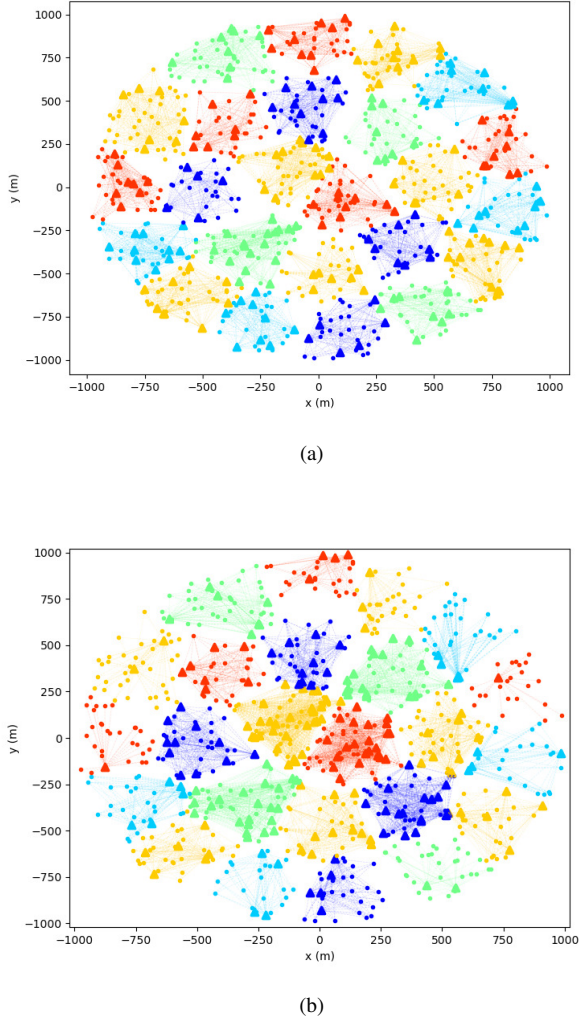


Fig. 1. **Visualization of  $C^2$  architectures with a constant user density but different BS densities.** Triangles are BSs. Circles are users. Each cluster is presented as a group of inter-connected nodes in the same color. (a)  $C^2$  architecture with a constant BS density. (b)  $C^2$  architecture with an inconstant BS density. BSs are centrally dense and peripherally sparse.

### B. Cluster Capacity Region of $C^2$ Architectures

The capacity region is one of the most important performance metrics for wireless networks, but its derivation is always complex and difficult. In this subsection, we will study the minimum and maximum values for  $C_j^\infty$ . Denote the maximum value of  $C_j^\infty$  as  $C_j^\infty|_{\max}$ , and the minimum value of  $C_j^\infty$  as  $C_j^\infty|_{\min}$ . To derive the expressions of  $C_j^\infty|_{\max}$  and  $C_j^\infty|_{\min}$ , concrete path-loss model should be given. In this paper, we consider a three-slope model [29], with path-loss parameters  $\theta$  and  $\alpha$  defined as

$$\theta = \begin{cases} 1, & d_{xy} > d_1, \\ d_1^{-1.5}, & d_0 < d_{xy} \leq d_1, \\ d_1^{-1.5} d_0^{-2}, & 0 < d_{xy} \leq d_0, \end{cases} \quad (22)$$

$$\alpha = \begin{cases} 3.5, & d_{xy} > d_1, \\ 2, & d_0 < d_{xy} \leq d_1, \\ 0, & 0 < d_{xy} \leq d_0, \end{cases}$$

where  $d_0$  and  $d_1$  can be interpreted as the near-field boundary and the far-field boundary, respectively.

According to our Corollary 1, both  $C_j^\infty|_{\max}$  and  $C_j^\infty|_{\min}$  can be determined if we find their corresponding BS locations. The process to determine  $C_j^\infty|_{\max}$  and  $C_j^\infty|_{\min}$  are elaborated as follows. Based on (13), we define

$$C_j^\infty = \log \Lambda_j, \quad (23)$$

where

$$\Lambda_j = \lim_{K_j, L_j \rightarrow \infty} \left[ \prod_{l=1}^{L_j} (1 + P \lambda_{lj}) \right]^{\frac{1}{L_j}}. \quad (24)$$

To determine the range of  $C_j^\infty$ , we start from analyzing  $\Lambda_j$ . Based on Corollary 1 and (23), we have

$$\frac{1}{\Lambda_j} = \frac{\int_{\mathbf{y} \in \mathcal{D}_0 \setminus \mathcal{D}_j} f(\mathbf{x}_{jl} - \mathbf{y}) d\mathbf{y}}{\int_{\mathbf{y} \in \mathcal{D}_0} f(\mathbf{x}_{jl} - \mathbf{y}) d\mathbf{y}} = 1 - \frac{\int_{\mathbf{y} \in \mathcal{D}_j} f(\mathbf{x}_{jl} - \mathbf{y}) d\mathbf{y}}{\int_{\mathbf{y} \in \mathcal{D}_0} f(\mathbf{x}_{jl} - \mathbf{y}) d\mathbf{y}}, \quad (25)$$

for some BS  $b_l$  with coordinates  $\mathbf{x}_{jl} \in \mathcal{D}_j$ . Then we define a function for all the BSs in  $\mathcal{D}_j$ , as

$$V_j(\mathbf{x}) = 1 - \frac{\int_{\mathbf{y} \in \mathcal{D}_j} f(\mathbf{x} - \mathbf{y}) d\mathbf{y}}{\int_{\mathbf{y} \in \mathcal{D}_0} f(\mathbf{x} - \mathbf{y}) d\mathbf{y}}, \quad \forall \mathbf{x} \in \mathcal{D}_j. \quad (26)$$

The range of  $\frac{1}{\Lambda_j}$  is a subset of the range of  $V_j(\mathbf{x})$ , and can be expressed as

$$V_j(\mathbf{x})|_{\min} \leq \frac{1}{\Lambda_j} \leq V_j(\mathbf{x})|_{\max}, \quad (27)$$

where  $V_j(\mathbf{x})|_{\min}$  and  $V_j(\mathbf{x})|_{\max}$  are the minimum value and maximum value of  $V_j(\mathbf{x})$ , respectively. The properties of  $V_j(\mathbf{x})|_{\min}$  and  $V_j(\mathbf{x})|_{\max}$  are summarized in the below two lemmas.

**Lemma 2:** Conditioning on a round network area with a constant user density, and a given three-slope path-loss model (22), the properties of  $V_j(\mathbf{x})|_{\min}$  are listed as follows:

- $V_j(\mathbf{x})|_{\min} \leq V_j(\mathbf{x}_{O_j})$ ,
- The upper bound of  $V_j(\mathbf{x})|_{\min}$  is

$$V_j(\mathbf{x})|_{\min} \leq \begin{cases} \frac{\frac{2}{3} R_j^{-1.5}}{d_1^{-1.5} \left( \frac{7}{6} + \ln \frac{d_1}{d_0} \right)}, & d_1 < R_j \leq 2R_0, \\ \frac{\ln \frac{d_1}{R_j} + \frac{2}{3}}{\ln \frac{d_1}{d_0} + \frac{7}{6}}, & d_0 < R_j \leq d_1, \\ 1 - \frac{R_j^2}{2d_0 \left( \ln \frac{d_1}{d_0} + \frac{7}{6} \right)}, & 0 < R_j \leq d_0. \end{cases} \quad (28)$$

*Proof:* Please see Appendix B. ■

Lemma 2 reveals that the upper bound of  $V_j(\mathbf{x})|_{\min}$  is achieved when  $\mathbf{x} = \mathbf{x}_{O_j}$ , which is the center point of  $\mathcal{D}_j$ . By substituting  $\mathbf{x} = \mathbf{x}_{O_j}$  into (26) and with further manipulation, the upper bound of  $V_j(\mathbf{x})|_{\min}$  is derived as (28) shown.

**Lemma 3:** Conditioning on a round network area with a constant user density, and a given three-slope path-loss model (22), the properties of  $V_j(\mathbf{x})|_{\max}$  are listed as follows:

- $V_j(\mathbf{x})|_{\max} = V_j(\mathbf{x}')$ , where  $\mathbf{x}'$  is the coordinates of the point located at the boundary of  $\mathcal{D}_j$  and closest to  $O_0$ .

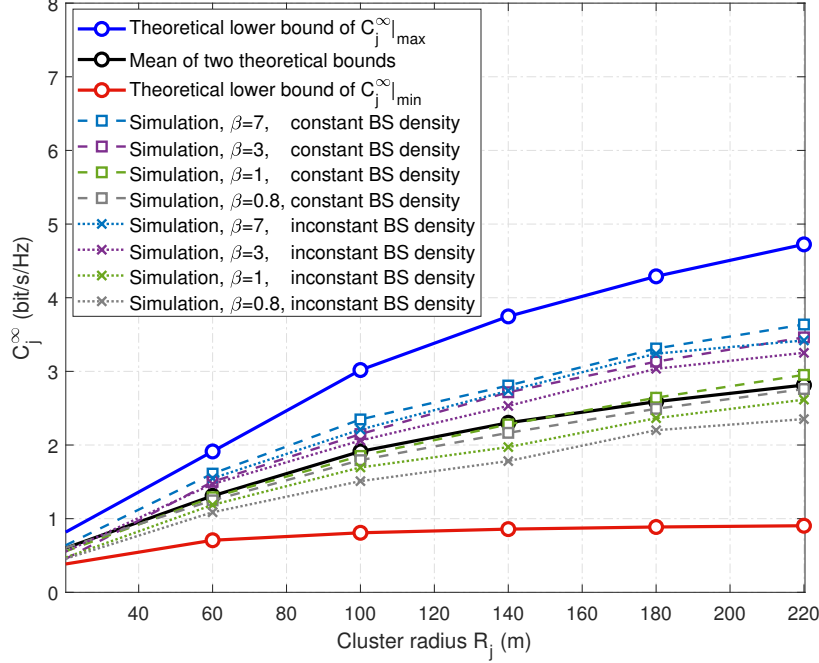


Fig. 2. **Theoretical and simulation results for the average cluster capacity per BS versus cluster radius with a constant user density.** Simulation results (8 dashed lines) contain the scenarios of constant and inconstant BS densities, and four different ratios between the number of users and the number of BSs ( $\beta = 0.8, 1, 3, 7$ ).

- The upper bound of  $V_j(\mathbf{x})|_{\max}$  is

$$V_j(\mathbf{x})|_{\max} \leq 1 - \frac{q(R_j)}{2\pi d_1^{-1.5} \left( \ln \frac{d_1}{d_0} + \frac{7}{6} \right)}, \quad (29)$$

where  $q(R_j) = \int_{\mathbf{y} \in \mathcal{D}_j} f(\mathbf{x}' - \mathbf{y}) d\mathbf{y}$  is an increasing function of  $R_j$ , and  $0 < q(R_j) \leq \pi d_1^{-1.5} \left( \ln \frac{d_1}{d_0} + \frac{7}{6} \right)$ .

- $0 < V_j(\mathbf{x})|_{\max} \leq 1$ .
- $V_j(\mathbf{x})|_{\max} \geq \frac{1}{2}$  for  $R_j \leq R_0/2$ .

*Proof:* Please see Appendix C. ■

Lemma 3 shows that  $V_j(\mathbf{x})|_{\max}$  is achieved when  $\mathbf{x} = \mathbf{x}'$ . Through substituting  $\mathbf{x} = \mathbf{x}'$  into (26) and with further manipulation, the upper bound of  $V_j(\mathbf{x})|_{\max}$  can be determined as (29) shown.

Since (27) is equivalent to

$$\frac{1}{V_j(\mathbf{x})|_{\max}} \leq \Lambda_j \leq \frac{1}{V_j(\mathbf{x})|_{\min}}, \quad (30)$$

the range of  $C_j^\infty$  can be expressed as

$$\log \frac{1}{V_j(\mathbf{x})|_{\max}} \leq C_j^\infty \leq \log \frac{1}{V_j(\mathbf{x})|_{\min}}, \quad (31)$$

which means

$$C_j^\infty|_{\min} = \log \frac{1}{V_j(\mathbf{x})|_{\max}}, \quad C_j^\infty|_{\max} = \log \frac{1}{V_j(\mathbf{x})|_{\min}}. \quad (32)$$

Combining (32) with Lemma 2 and Lemma 3, we get the following theorem for  $C_j^\infty|_{\min}$  and  $C_j^\infty|_{\max}$ :

*Theorem 2 (Average cluster capacity region):* Conditioning on a round network area with a constant user density, and a

given three-slope path-loss model (22), the lower bound of  $C_j^\infty|_{\max}$  for a round cluster can be determined by

$$C_j^\infty|_{\max} \geq \begin{cases} \log \left[ R_j^{-1.5} d_1^{-1.5} \left( \frac{3}{2} \ln \frac{d_1}{d_0} + \frac{7}{4} \right) \right], & d_1 < R_j \leq 2R_0, \\ \log \left( \ln \frac{d_1}{d_0} + \frac{7}{6} \right) - \log \left( \ln \frac{d_1}{R_j} + \frac{2}{3} \right), & d_0 < R_j \leq d_1, \\ -\log \left[ 1 - \frac{R_j^2}{2d_0^2 \left( \ln \frac{d_1}{d_0} + \frac{7}{6} \right)} \right], & 0 < R_j \leq d_0. \end{cases} \quad (33)$$

The lower bound of  $C_j^\infty|_{\min}$  can be determined by

$$C_j^\infty|_{\min} \geq \log \frac{2\pi d_1^{-1.5} \left( \ln \frac{d_1}{d_0} + \frac{7}{6} \right)}{2\pi d_1^{-1.5} \left( \ln \frac{d_1}{d_0} + \frac{7}{6} \right) - q(R_j)}. \quad (34)$$

It can be observed that both the bounds for  $C_j^\infty|_{\max}$  and  $C_j^\infty|_{\min}$  are increasing functions of the cluster radius  $R_j$ , consistent with the aforementioned result that  $C_j^\infty$  and cluster area  $|\mathcal{D}_j|$  are positively correlated. The physical insight is that the more nodes in a cluster performing coordinated communications, the larger cluster capacity achieved. Moreover, by substituting  $R_j^*$  for  $R_j$  in (33) and (34), we can obtain the lower bounds for  $C_j^\infty|_{\max}$  and  $C_j^\infty|_{\min}$  of a  $C^2$  architecture. As such, Theorem 2 provides a substantially simplified way to determine the region of average cluster capacity, reducing the complexity from high-dimensional matrix manipulation (shown as (9)) to pure numerical calculation. In practice, Theorem 2 can be applied for evaluating real-world networks, whose region can be regarded as round and users are distributed with a constant density.

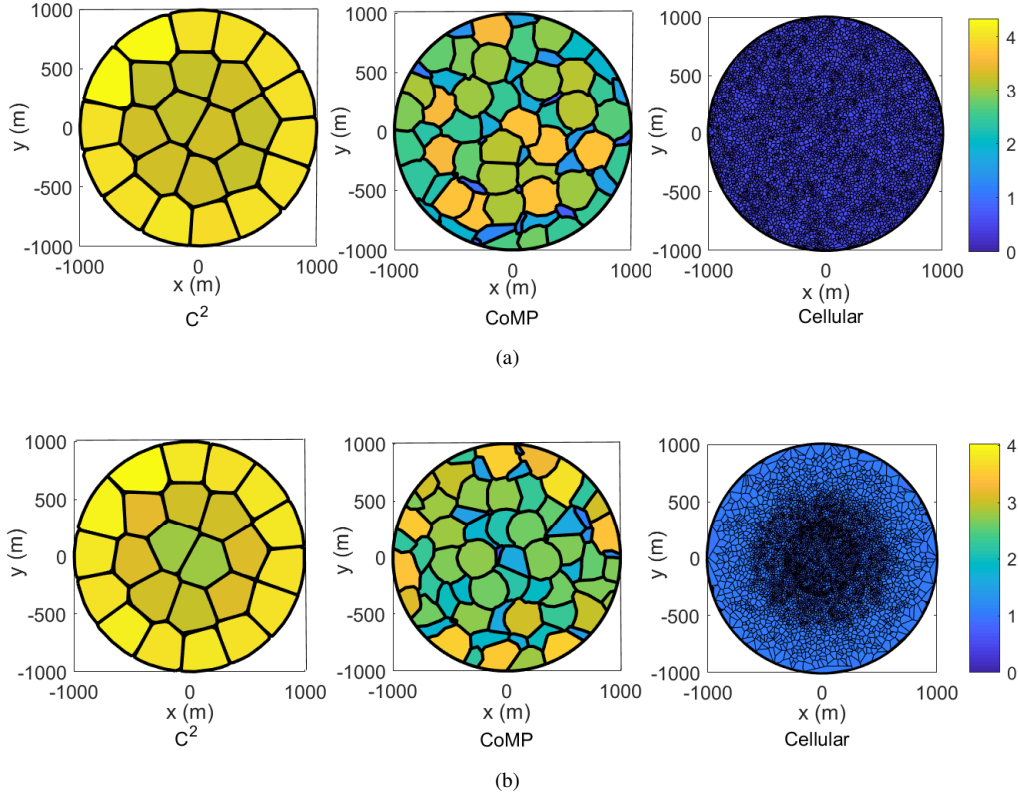


Fig. 3. Heatmaps of the average cluster capacity per BS of every cluster in  $C^2$ , CoMP, and cellular architectures. The region circled with a black boundary is a cluster.  $R_0 = 1000$  m,  $\beta = 3$ ,  $R_{Th} = 175$  m. Users are distributed with a constant density  $\rho_u = 6 \times 10^{-3} \text{ m}^{-2}$ . Two types of BS distributions are considered. (a) BSs are distributed with a constant density. (b) BSs are distributed with an inconstant density, which is centrally dense and peripherally sparse.

To verify Theorem 2, we plot both of our derived theoretical bounds and a series of simulated  $C_j^\infty$  in Fig. 2. We set the network radius as  $R_0 = 1000$  m, changing the cluster radius  $R_j$  from 20 m to 220 m, and plot the lower bounds of  $C_j^\infty|_{\max}$  and  $C_j^\infty|_{\min}$  for each  $R_j$  as a blue curve and a red curve, respectively. The arithmetic mean of these two bounds is plotted as a black curve. Note that Theorem 2 only restricts the user density as a constant, but does not have any constraint on BS distributions. We fix the user density as  $\rho_u = 6 \times 10^{-3} \text{ m}^{-2}$ , and generate a series of  $C^2$  architectures with different parameter settings on BS distributions, to plot the simulated  $C_j^\infty$  according to its original definition (9). The parameter settings include four values of  $\beta$  and two kinds of BS densities, one is constant and the other is centrally dense and peripherally sparse (please refer to Section IV-A for details). It can be observed that the theoretical bounds of  $C_j^\infty|_{\max}$  and  $C_j^\infty|_{\min}$  indeed bound the range of simulated  $C_j^\infty$  with various parameter settings, and thus can be directly utilized to evaluate the network performance in practice. Moreover, the simulated  $C_j^\infty$  is positively correlated to the ratio  $\beta$  for a given BS distribution;  $C_j^\infty$  approaches the bound of  $C_j^\infty|_{\max}$  as  $\beta$  increases, while approaches the bound of  $C_j^\infty|_{\min}$  as  $\beta$  decreases. It means the bound of  $C_j^\infty|_{\max}$  becomes tighter as  $\beta$  increases, and the bound of  $C_j^\infty|_{\min}$  is tighter as  $\beta$  decreases. This is because the larger  $\beta$  corresponds to the fewer BSs, and  $C_j^\infty$  is inversely proportional to the number of BSs as

defined in (9). Another observation that we wish to point out is that, the simulated  $C_j^\infty$  approaches the black curve as  $\beta$  approaches 1. This implies that the average value of the two theoretical bounds can be regarded as an approximation on  $C_j^\infty$  for real-world networks with similar numbers of BSs and users.

## V. PERFORMANCE COMPARISON ACROSS $C^2$ , CoMP, AND CELLULAR ARCHITECTURES

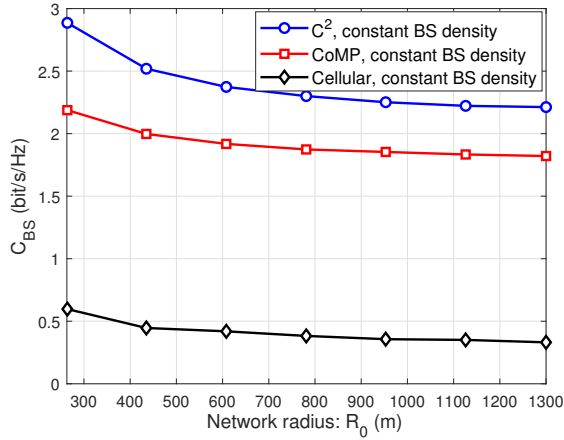
In this section, we will compare the performance of three network architectures, including our proposed  $C^2$  architecture and two conventional BS-centric architectures: CoMP and cellular.

In simulation, we set up a round network region with radius  $R_0 = 1000$  m, where we generate users and BSs with location coordinates randomly chosen from continuous uniform distributions, with densities of  $\rho_u = 6 \times 10^{-3} \text{ m}^{-2}$  and  $\rho_b = \rho_u/\beta$ , respectively. Parameters of the near-field boundary and the far-field boundary are chosen as  $d_0 = 10$  m and  $d_1 = 50$  m, respectively. The way to emulate three different architectures are briefly introduced below:

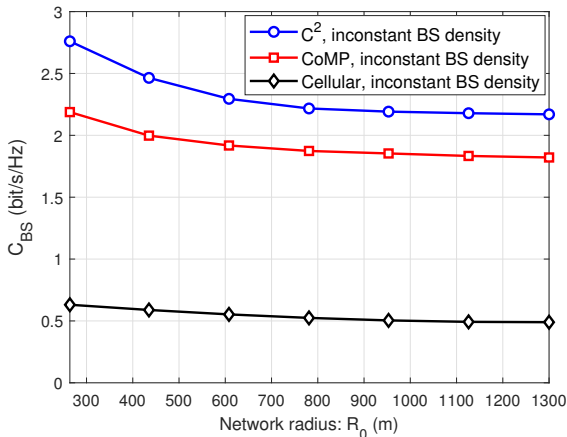
- The cellular architecture is BS-centric and emulated through each user attaching to its nearest BS, forming the Voronoi tessellation [32].
- The CoMP architecture is an enhanced version of the cellular architecture, and is BS-centric as well. We emulate

it through choosing a datum BS randomly, assembling surrounding BSs within distance  $R_{CoMP}$  to this datum as a cluster. Then we choose another datum BS randomly in the remaining BSs and repeat the clustering steps until no BSs remain. Each user attaches to its nearest BS and thus belongs to the cluster this BS is located in.

- The  $C^2$  architecture can be plotted directly based on our derived optimal cluster number  $M^*$  and optimal cluster radius  $R_j^*$  with a given cluster radius threshold  $R_{Th}$ <sup>1</sup>. For fair comparisons,  $R_{CoMP}$  in CoMP is chosen to be the same as  $R_j^*$  in  $C^2$ . We name the coverage map of the  $C^2$  architecture ‘ $C^2$  tessellation’.



(a)



(b)

Fig. 4. Comparison across  $C^2$ , CoMP, and cellular architectures in terms of the overall network average capacity per BS versus network radius.  $\beta = 2$ ,  $R_{Th} = 100$  m. Users are distributed with a constant density  $\rho_u = 6 \times 10^{-3} \text{ m}^{-2}$ . Two different BS distributions are considered. (a) BSs are distributed with a constant density. (b) BSs are distributed with an inconstant density, which is centrally dense and peripherally sparse.

In Fig. 3, we plot the heatmaps of  $C_j^\infty$  of every cluster in  $C^2$ , CoMP, and cellular architectures to compare their

<sup>1</sup>Clusters are arranged according to the circle packing in a circle. There may be a few nodes not belonging to any cluster. For these nodes, we perform a fine-grained tuning in simulation by assigning each node to the cluster with minimum distance between the cluster center and this node.

performance. Users are distributed with a constant density  $\rho_u = 6 \times 10^{-3} \text{ m}^{-2}$ . Two types of BS distributions are considered, including the constant density and the inconstant density, shown in Fig. 3(a) and Fig. 3(b), respectively. The inconstant density case refers to BSs deployed centrally dense and peripherally sparse, and please refer to Section IV-A for details. It can be observed that the  $C^2$  architecture is not over-reliant on BS distributions: the optimal number of clusters  $M^* = 24$ , and the size of each cluster is the same under different BS distributions. In addition, the  $C^2$  architecture has the highest  $C_j^\infty$  compared to its two alternatives, guaranteeing that each BS/user has the highest communication quality. Different from  $C^2$ , CoMP and cellular are BS-centric architectures, and thus exhibit different forms under different BS distributions in Fig. 3. Compared to  $C^2$ , CoMP has a larger difference in cluster size and  $C_j^\infty$ , which implies that it can not guarantee a sufficient communication quality everywhere. As for the cellular architecture, each cluster corresponds to the coverage area of a single BS. Its cluster area is the smallest, and its  $C_j^\infty$  is the lowest. As we previously analyzed, cellular can be regarded as an extreme case of our  $C^2$  architecture, with the number of clusters taking its maximum value  $L$ . As a brief summary, the  $C^2$  architecture provides the highest average cluster capacity per BS/user, and is also the most robust one. Even though the BS distribution is changed, the clusters under the  $C^2$  architecture do not change.

After evaluating the cluster performance, we take a step further to evaluate the performance of the overall network. The overall network average capacity per BS, denoted by  $C_{BS}$ , can be derived based on the average cluster capacity per BS  $C_j^\infty$  as

$$C_{BS} = \frac{\sum_{j=1}^M C_j^\infty L_j}{L}. \quad (35)$$

The overall network average capacity per user is  $C_u = \frac{C_{BS}}{\beta}$ , only with a difference of constant  $\beta$  compared to  $C_{BS}$ . Here, we choose  $C_{BS}$  as the performance metric without losing the generality, since  $C_u$  and  $C_{BS}$  have the same trends. A comparison across three network architectures in terms of  $C_{BS}$  versus the network radius  $R_0$  is shown in Fig. 4. Our simulation results show that in the case of constant BS density,  $C^2$  outperforms CoMP and cellular with gains of at least 21.2% and 383%, respectively. In the case of inconstant BS density, which is centrally dense and peripherally sparse (please refer to Section IV-A for details),  $C^2$  outperforms CoMP and cellular with gains of at least 17.5% and 315%, respectively.

## VI. CONCLUSION

In this paper, we proposed a  $C^2$  architecture for future wireless networking. It guarantees high capacity for each BS and each user, and exhibits superior scalability with minimal signaling overhead simultaneously. The  $C^2$  architecture is designed based on our average cluster capacity theorem, which eliminates high-dimensional matrix calculations and is adaptive to different networks. The  $C^2$  architecture has excellent generality; both the commercialized cellular architecture and the idealized fully coordinated architecture are its extreme

cases. Simulation results showed that the  $C^2$  architecture has the highest overall network average capacity per BS (or per user). It outperforms cellular and CoMP architectures with performance gains of at least 300% and 17.5%, respectively. Last but not the least, the  $C^2$  architecture is fixed if the user distribution is fixed, not over-reliant on BS distributions. On one hand, it means that  $C^2$  has excellent robustness with a given user distribution, in the sense that its clusters will not change even if the BS distribution is changed. On the other hand, it implies the user-side information should not be ignored and deserves more attention in future network designs. All of these findings can be applied in a wide variety of wireless scenarios for networking architecture designs, such as 6G, Wi-Fi, vehicle to everything (V2X) and Industry 4.0, etc.

#### ACKNOWLEDGMENTS

L. Yang thanks Prof. Mayank Bakshi and Dr. Yuhao Liu for fruitful discussions and support on this article.

#### APPENDIX A PROOF OF LEMMA 1

Based on (1), the channel gain matrix of cluster  $j$  can be written as

$$\mathbf{H}_j = \mathbf{L}_j \circ \mathbf{G}_j, \quad (36)$$

where “ $\circ$ ” denotes the Hadamard product.  $\mathbf{G}_j$  is the small-scale fading matrix, which is complex Gaussian.  $\mathbf{L}_j$  is the path-loss matrix, and is deterministic. The equivalent channel gain matrix  $\tilde{\mathbf{H}}_j$  can be written as

$$\tilde{\mathbf{H}}_j = \frac{1}{\sqrt{K_j}} \sqrt{K_j} (N_0 \mathbf{I} + \boldsymbol{\Sigma}_j)^{-\frac{1}{2}} \mathbf{L}_j \circ \mathbf{G}_j = \frac{1}{\sqrt{K_j}} \mathbf{T}_j \circ \mathbf{G}_j \quad (37)$$

where

$$\mathbf{T}_j = \sqrt{K_j} (N_0 \mathbf{I} + \boldsymbol{\Sigma}_j)^{-\frac{1}{2}} \mathbf{L}_j. \quad (38)$$

The  $(l, k)$ -th entry of  $\mathbf{T}_j$  is given by

$$[\mathbf{T}_j]_{l,k} = \sqrt{\frac{K_j \times \ell_{jlk}^2}{N_0 + \sum_{u \in \mathcal{U} \setminus C_j} \ell_{jlk}^2 P}}, \quad (39)$$

whose value is limited. Then the matrix  $\tilde{\mathbf{H}}_j \tilde{\mathbf{H}}_j^H$  can be written as

$$\tilde{\mathbf{H}}_j \tilde{\mathbf{H}}_j^H = \frac{1}{K_j} \mathbf{T}_j \circ \mathbf{G}_j \mathbf{G}_j^H \circ \mathbf{T}_j^H. \quad (40)$$

Since the matrix  $\mathbf{T}_j$  is determined, and its entries can be regarded as fixed parameters, our objective becomes to investigate the asymptotic properties of the complex random matrix  $\frac{1}{K_j} \mathbf{G}_j \mathbf{G}_j^H$  as  $K_j, L_j \rightarrow \infty$ ,  $\frac{K_j}{L_j} = \beta_j \in (0, \infty)$ .

Denote  $\mathbf{Q} = \frac{1}{K_j} \mathbf{G}_j \mathbf{G}_j^H$ , and  $\hat{\mathbf{Q}} = \text{diag}(q_1, q_2, \dots, q_{L_j})$ , with  $q_l = \mathbb{E}[\frac{1}{K_j} \sum_{k=1}^{K_j} g_{jlk} \bar{g}_{jlk}]$ , ( $l = 1, 2, \dots, L_j$ ). In the following, we will prove  $\mathbf{Q}$  approaches  $\hat{\mathbf{Q}}$  as  $K_j, L_j \rightarrow \infty$ ,  $\frac{K_j}{L_j} = \beta_j \in (0, \infty)$ , by analyzing its diagonal entries and off-diagonal entries, respectively. The mathematical tool we

mainly use is the concentration inequality: if random variables  $\{X_i\}_{i=1}^\infty \stackrel{i.i.d.}{\sim} \mathcal{N}(0, 1)$ , then  $\sum_{i=1}^n X_i^2 \sim \mathcal{X}_n^2$ , and

$$\begin{aligned} \mathbb{P} \left( \left| \frac{1}{n} \sum_{i=1}^n X_i^2 - 1 \right| \geq \epsilon \right) &= \mathbb{P} \left( \left| \frac{1}{n} \mathcal{X}_n^2 - 1 \right| \geq \epsilon \right) \\ &\leq 2 \exp \left( -\frac{1}{8} \epsilon^2 n \right), \end{aligned} \quad (41)$$

where  $\mathcal{X}_n^2$  denotes the chi-square distribution with  $n$  degrees of freedom.

#### A. Diagonal Entries Analysis

Define complex random variables  $\{Z_i = X_i + iY_i\}_{i=1}^\infty$ , where  $X_i, Y_i \stackrel{i.i.d.}{\sim} \mathcal{N}(0, 1)$ ,  $X_i$  and  $Y_i$  are pairwise independent.

$$\begin{aligned} &\mathbb{P} \left( \left| \frac{1}{n} \sum_{i=1}^n Z_i \bar{Z}_i - \mathbb{E} \left[ \frac{1}{n} \sum_{i=1}^n Z_i \bar{Z}_i \right] \right| \geq \epsilon \right) \\ &= \mathbb{P} \left( \left| \frac{1}{n} \sum_{i=1}^n (X_i^2 + Y_i^2) - 2 \right| \geq \epsilon \right) \\ &\leq \mathbb{P} \left( \left| \frac{1}{n} \sum_{i=1}^n X_i^2 - 1 \right| \geq \frac{\epsilon}{2} \right) + \mathbb{P} \left( \left| \frac{1}{n} \sum_{i=1}^n Y_i^2 - 1 \right| \geq \frac{\epsilon}{2} \right) \\ &\leq 4 \exp \left( -\frac{1}{32} \epsilon^2 n \right). \end{aligned} \quad (42)$$

Therefore, for the diagonal entries, we have

$$\mathbb{P} \left( \left| [\mathbf{Q}]_{l,l} - [\hat{\mathbf{Q}}]_{l,l} \right| \geq \epsilon \right) \leq 4 \exp \left( -\frac{1}{32} \epsilon^2 K_j \right), \quad (43)$$

where  $l = 1, 2, \dots, L_j$ .

#### B. Off-Diagonal Entries Analysis

Consider  $\{U_i = W_i + iV_i\}_{i=1}^\infty$ ,  $\{Z_i = X_i + iY_i\}_{i=1}^\infty$ , where  $W_i, V_i, X_i, Y_i \stackrel{i.i.d.}{\sim} \mathcal{N}(0, 1)$ , and  $W_i, V_i, X_i, Y_i$  are pairwise independent.

$$\begin{aligned} &\mathbb{P} \left( \left| \frac{1}{n} \sum_{i=1}^n U_i \bar{Z}_i \right| \geq \epsilon \right) \\ &= \mathbb{P} \left( \left| \frac{1}{n} \left[ \left( \sum_{i=1}^n W_i X_i + V_i Y_i \right) + i \left( \sum_{i=1}^n V_i X_i - W_i Y_i \right) \right] \right| \geq \epsilon \right) \\ &\leq \mathbb{P} \left( \left| \frac{1}{n} \sum_{i=1}^n W_i X_i \right| \geq \frac{\sqrt{2}\epsilon}{4} \right) + \mathbb{P} \left( \left| \frac{1}{n} \sum_{i=1}^n V_i Y_i \right| \geq \frac{\sqrt{2}\epsilon}{2} \right) + \\ &\quad \mathbb{P} \left( \left| \frac{1}{n} \sum_{i=1}^n V_i X_i \right| \geq \frac{\sqrt{2}\epsilon}{4} \right) + \mathbb{P} \left( \left| \frac{1}{n} \sum_{i=1}^n W_i Y_i \right| \geq \frac{\sqrt{2}\epsilon}{2} \right) \\ &= 4 \mathbb{P} \left( \left| \frac{1}{n} \sum_{i=1}^n W_i X_i \right| \geq \frac{\sqrt{2}\epsilon}{4} \right). \end{aligned} \quad (44)$$

Deriving the above probability is equivalent to the following problem: If  $\{X_i\}_{i=1}^\infty \stackrel{i.i.d.}{\sim} \mathcal{N}(0, 1)$ ,  $\{Y_i\}_{i=1}^\infty \stackrel{i.i.d.}{\sim} \mathcal{N}(0, 1)$ ,  $X_i$  and  $Y_i$  are pairwise independent, what's the probability

of  $\mathbb{P}\left(\left|\frac{1}{n}\sum_{i=1}^n X_i Y_i\right| \geq \epsilon\right)$ . Then we perform the following transformation:

$$\begin{aligned} \sum_{i=1}^n X_i Y_i &= \frac{1}{2} \left[ \sum_{i=1}^n (X_i + Y_i)^2 - \sum_{i=1}^n (X_i^2 + Y_i^2) \right] \\ &= \frac{1}{2} \left[ \left( \sum_{i=1}^n (X_i + Y_i)^2 - 2n \right) - \left( \sum_{i=1}^n X_i^2 - n \right) - \left( \sum_{i=1}^n Y_i^2 - n \right) \right], \end{aligned} \quad (45)$$

and thus

$$\begin{aligned} &\mathbb{P}\left(\left|\frac{1}{n}\sum_{i=1}^n X_i Y_i\right| \geq \epsilon\right) \\ &= \mathbb{P}\left[\left|\left(\frac{1}{n}\sum_{i=1}^n \left(\frac{X_i + Y_i}{\sqrt{2}}\right)^2 - 1\right) - \left(\frac{1}{2n}\sum_{i=1}^n X_i^2 + \frac{1}{2n}\sum_{i=1}^n Y_i^2 - 1\right)\right| \geq \epsilon\right] \\ &\leq \mathbb{P}\left(\left|\frac{1}{n}\sum_{i=1}^n \left(\frac{X_i + Y_i}{\sqrt{2}}\right)^2 - 1\right| \geq \frac{\epsilon}{2}\right) + \\ &\quad \mathbb{P}\left(\left|\frac{1}{2n}\sum_{i=1}^n X_i^2 + \frac{1}{2n}\sum_{i=1}^n Y_i^2 - 1\right| \geq \frac{\epsilon}{2}\right). \end{aligned} \quad (46)$$

Since  $X_i + Y_i \sim \mathcal{N}(0, 2)$ ,  $\frac{X_i + Y_i}{\sqrt{2}} \sim \mathcal{N}(0, 1)$ , and  $X_i, Y_i$  are pairwise independent, then we have  $\sum_{i=1}^n \left(\frac{X_i + Y_i}{\sqrt{2}}\right)^2 \sim \chi_n^2$ . Moreover,  $\frac{1}{2n}(\sum_{i=1}^n X_i^2 + \sum_{i=1}^n Y_i^2) \sim \chi_{2n}^2$ . According to (41), we have

$$\begin{aligned} &\mathbb{P}\left(\left|\frac{1}{n}\sum_{i=1}^n \left(\frac{X_i + Y_i}{\sqrt{2}}\right)^2 - 1\right| \geq \frac{\epsilon}{2}\right) \leq 2 \exp\left(-\frac{1}{32}\epsilon^2 n\right), \\ &\mathbb{P}\left(\left|\frac{1}{2n}\sum_{i=1}^n (X_i^2 + Y_i^2) - 1\right| \geq \frac{\epsilon}{2}\right) \leq 2 \exp\left(-\frac{1}{16}\epsilon^2 n\right). \end{aligned} \quad (47)$$

Thus

$$\begin{aligned} \mathbb{P}\left(\left|\frac{1}{n}\sum_{i=1}^n X_i Y_i\right| \geq \epsilon\right) &\leq 2 \exp\left(-\frac{1}{32}\epsilon^2 n\right) + 2 \exp\left(-\frac{1}{16}\epsilon^2 n\right) \\ &\leq 4 \exp\left(-\frac{1}{32}\epsilon^2 n\right), \end{aligned} \quad (48)$$

and

$$\begin{aligned} \mathbb{P}\left(\left|\frac{1}{n}\sum_{i=1}^n U_i \bar{Z}_i\right| \geq \epsilon\right) &\leq 4 \mathbb{P}\left(\left|\frac{1}{n}\sum_{i=1}^n W_i X_i\right| \geq \frac{\sqrt{2}\epsilon}{4}\right) \\ &\leq 16 \exp\left(-\frac{1}{256}\epsilon^2 n\right). \end{aligned} \quad (49)$$

Therefore, for the off-diagonal entries, we have

$$\mathbb{P}\left(\left|[Q]_{l,k} - [\hat{Q}]_{l,k}\right| \geq \epsilon\right) \leq 16 \exp\left(-\frac{1}{256}\epsilon^2 K_j\right), \quad (l \neq k). \quad (50)$$

In summary, we have

$$\begin{aligned} \mathbb{P}\left(\|Q - \hat{Q}\|_\infty \geq \epsilon\right) &= \lim_{\substack{K_j, L_j \rightarrow \infty \\ K_j / L_j = \beta_j}} \mathbb{P}\left(\max_{l,k} \left|[Q]_{l,k} - [\hat{Q}]_{l,k}\right| \geq \epsilon\right) \\ &= \lim_{\substack{K_j, L_j \rightarrow \infty \\ K_j / L_j = \beta_j}} \mathbb{P}\left(\bigcup_{l,k} \left|[Q]_{l,k} - [\hat{Q}]_{l,k}\right| \geq \epsilon\right) \\ &\leq \lim_{\substack{K_j, L_j \rightarrow \infty \\ K_j / L_j = \beta_j}} \mathbb{P}\left(\max_{l,k} \left|[Q]_{l,k} - [\hat{Q}]_{l,k}\right| \geq \epsilon\right) \\ &\leq \lim_{\substack{K_j, L_j \rightarrow \infty \\ K_j / L_j = \beta_j}} 16L_j^2 \exp\left(-\frac{1}{256}\epsilon^2 K_j\right) = 0, \end{aligned} \quad (51)$$

which means  $\lim_{K_j, L_j \rightarrow \infty, K_j / L_j = \beta_j} Q \xrightarrow{p} \hat{Q}$ . Combining this result with (39) and (40), we have

$$\begin{aligned} &\lim_{\substack{K_j, L_j \rightarrow \infty \\ K_j / L_j = \beta_j}} \tilde{H}_j \tilde{H}_j^H \xrightarrow{p} \text{diag}\left(\frac{\sum_{u_k \in \mathcal{U}_j} \ell_{j1k}^2}{N_0 + \sum_{u_\kappa \in \mathcal{U} \setminus \mathcal{C}_j} \ell_{j1\kappa}^2 P}, \right. \\ &\quad \left. \frac{\sum_{u_k \in \mathcal{U}_j} \ell_{j2k}^2}{N_0 + \sum_{u_\kappa \in \mathcal{U} \setminus \mathcal{C}_j} \ell_{j2\kappa}^2 P}, \dots, \frac{\sum_{u_k \in \mathcal{U}_j} \ell_{jL_j k}^2}{N_0 + \sum_{u_\kappa \in \mathcal{U} \setminus \mathcal{C}_j} \ell_{jL_j \kappa}^2 P}\right). \end{aligned} \quad (52)$$

The proof of Lemma 1 is completed.

## APPENDIX B PROOF OF LEMMA 2

Based on the fact that  $V_j(\mathbf{x})|_{\min}$  is less than or equal to  $V_j(\mathbf{x}_{O_j})$ , we have

$$\begin{aligned} V_j(\mathbf{x})|_{\min} &\leq V_j(\mathbf{x}_{O_j}) \\ &= \frac{\int_{\mathbf{y} \in \mathcal{D}_0 - \mathcal{D}_j} f(\mathbf{x}_{O_j} - \mathbf{y}) d\mathbf{y}}{\int_{\mathbf{y} \in \mathcal{D}_0} f(\mathbf{x}_{O_j} - \mathbf{y}) d\mathbf{y}} \\ &\leq \frac{\int_{\mathbf{y} \in \mathcal{D}_0 - \mathcal{D}_j} f(\mathbf{x}_{O_j} - \mathbf{y}) d\mathbf{y} \Big|_{\mathcal{D}_0 \rightarrow \infty}}{\int_{\mathbf{y} \in \mathcal{D}_0} f(\mathbf{x}_{O_j} - \mathbf{y}) d\mathbf{y} \Big|_{\mathcal{D}_0 \rightarrow \infty}}, \end{aligned} \quad (53)$$

where the denominator can be calculated as

$$\int_{\mathbf{y} \in \mathcal{D}_0} f(\mathbf{x}_{O_j} - \mathbf{y}) d\mathbf{y} \Big|_{\mathcal{D}_0 \rightarrow \infty} = 2\pi \rho_u d_1^{-1.5} \left(\frac{7}{6} + \ln \frac{d_1}{d_0}\right), \quad (54)$$

and the numerator is derived as

$$\begin{aligned} &\int_{\mathbf{y} \in \mathcal{D}_0 - \mathcal{D}_j} f(\mathbf{x}_{O_j} - \mathbf{y}) d\mathbf{y} \Big|_{\mathcal{D}_0 \rightarrow \infty} = \\ &\begin{cases} \frac{4}{3}\pi \rho_u R_j^{-1.5}, & d_1 < R_j \leq 2R_0, \\ 2\pi \rho_u d_1^{-1.5} \left(\ln \frac{d_1}{R_j} + \frac{2}{3}\right), & d_0 < R_j \leq d_1, \\ 2\pi \rho_u d_1^{-1.5} \left[\frac{1}{2} \left(1 - \frac{R_j^2}{d_0^2}\right) + \ln \frac{d_1}{d_0} + \frac{2}{3}\right], & 0 < R_j \leq d_0. \end{cases} \end{aligned} \quad (55)$$

Thus,

$$V_j(\mathbf{x})|_{\min} \leq \begin{cases} \frac{\frac{2}{3}R_j^{-1.5}}{d_1^{-1.5} \left(\frac{7}{6} + \ln \frac{d_1}{d_0}\right)}, & d_1 < R_j \leq 2R_0, \\ \frac{\ln \frac{d_1}{R_j} + \frac{2}{3}}{\ln \frac{d_1}{d_0} + \frac{2}{6}}, & d_0 < R_j \leq d_1, \\ 1 - \frac{R_j^2}{2d_0^2 \left(\ln \frac{d_1}{d_0} + \frac{7}{6}\right)}, & 0 < R_j \leq d_0. \end{cases} \quad (56)$$

The proof of Lemma 2 is completed.

APPENDIX C  
PROOF OF LEMMA 3

Denote  $F_j(\mathbf{x}) = \int_{\mathbf{y} \in \mathcal{D}_j} f(\mathbf{x} - \mathbf{y}) d\mathbf{y}$ , and  $F(\mathbf{x}) = \int_{\mathbf{y} \in \mathcal{D}_0} f(\mathbf{x} - \mathbf{y}) d\mathbf{y}$ , so that

$$V_j(\mathbf{x}) = 1 - \frac{F_j(\mathbf{x})}{F(\mathbf{x})}, \quad \forall \mathbf{x} \in \mathcal{D}_j. \quad (57)$$

It can be obtained that  $\forall \mathbf{x} \in \mathcal{D}_j$ ,  $F_j(\mathbf{x})$  is a constant for  $R_0 \leq \frac{d_0}{2}$ .  $F_j(\mathbf{x})|_{\min} = F_j(\mathbf{x}') = \int_{\mathbf{y} \in \mathcal{D}_j} f(\mathbf{x}' - \mathbf{y}) d\mathbf{y}$  for  $R_0 > \frac{d_0}{2}$ , since  $F_j(\mathbf{x})$  decreases as the distance between  $\mathbf{x}$  and  $\mathbf{x}_{O_j}$  increases. Moreover,  $\forall \mathbf{x} \in \mathcal{D}_j$ ,  $F(\mathbf{x})|_{\max} = F(\mathbf{x}') = \int_{\mathbf{y} \in \mathcal{D}_0} f(\mathbf{x}' - \mathbf{y}) d\mathbf{y}$  since  $F(\mathbf{x})$  decreases as the distance between  $\mathbf{x}$  and  $\mathbf{x}_{O_0}$  increases. Thus,  $V_j(\mathbf{x})|_{\max} = 1 - \frac{F_j(\mathbf{x}')}{F(\mathbf{x}')} = V_j(\mathbf{x}')$ . Define

$$q(R_j) = \int_{\mathbf{y} \in \mathcal{D}_j} f(\mathbf{x}' - \mathbf{y}) d\mathbf{y},$$

we have

$$\begin{aligned} V_j(\mathbf{x})|_{\max} &= \frac{\int_{\mathbf{y} \in \mathcal{D}_0 - \mathcal{D}_j} f(\mathbf{x}' - \mathbf{y}) d\mathbf{y}}{\int_{\mathbf{y} \in \mathcal{D}_0} f(\mathbf{x}' - \mathbf{y}) d\mathbf{y}} \\ &\leq \frac{\int_{\mathbf{y} \in \mathcal{D}_0 - \mathcal{D}_j} f(\mathbf{x}' - \mathbf{y}) d\mathbf{y} \Big|_{\mathcal{D}_0 \rightarrow \infty}}{\int_{\mathbf{y} \in \mathcal{D}_0} f(\mathbf{x}' - \mathbf{y}) d\mathbf{y} \Big|_{\mathcal{D}_0 \rightarrow \infty}} \\ &= 1 - \frac{q(R_j)}{2\pi d_1^{-1.5} \left( \ln \frac{d_1}{d_0} + \frac{7}{6} \right)}. \end{aligned}$$

It can be derived that  $\frac{d}{dR_j} q(R_j) > 0$ , which means  $q(R_j)$  is an increasing function of  $R_j$ . Thus, the lower bound and upper bound of  $q(R_j)$  can be determined as  $R_j \rightarrow 0$  and  $R_j \rightarrow +\infty$ , respectively, as

$$\begin{aligned} q(R_j) &\geq \lim_{R_j \rightarrow 0} \int_{\mathbf{y} \in \mathcal{D}_j} f(\mathbf{x}' - \mathbf{y}) d\mathbf{y} = \lim_{R_j \rightarrow 0} \pi R_j^2 d_1^{-1.5} d_0^{-2} = 0, \\ q(R_j) &\leq \lim_{R_j \rightarrow \infty} \int_{\mathbf{y} \in \mathcal{D}_j} f(\mathbf{x}' - \mathbf{y}) d\mathbf{y} = \pi d_1^{-1.5} \left( \ln \frac{d_1}{d_0} + \frac{7}{6} \right). \end{aligned}$$

As such,

$$\frac{1}{2} \leq 1 - \frac{q(R_j)}{2\pi d_1^{-1.5} \left( \ln \frac{d_1}{d_0} + \frac{7}{6} \right)} \leq 1,$$

which means

$$0 < V_j(\mathbf{x})|_{\max} \leq 1,$$

Moreover, if  $R_0 \geq 2R_j$ , it can be derived that

$$\begin{aligned} V_j(\mathbf{x})|_{\max} &= \frac{\int_{\mathbf{y} \in \mathcal{D}_j} f(\mathbf{x}' - \mathbf{y}) d\mathbf{y} + \int_{\mathbf{y} \in \mathcal{D}_0 - 2\mathcal{D}_j} f(\mathbf{x}' - \mathbf{y}) d\mathbf{y}}{2 \int_{\mathbf{y} \in \mathcal{D}_j} f(\mathbf{x}' - \mathbf{y}) d\mathbf{y} + \int_{\mathbf{y} \in \mathcal{D}_0 - 2\mathcal{D}_j} f(\mathbf{x}' - \mathbf{y}) d\mathbf{y}} \\ &\geq \frac{q(R_j)}{2q(R_j)} = \frac{1}{2}. \end{aligned}$$

The proof of Lemma 3 is completed.

REFERENCES

- [1] R. Li *et al.*, "Network 2030 - A Blueprint of Technology, Applications and Market Drivers Towards the Year 2030 and Beyond," International Telecommunications Union (ITU), White Paper, May 2019. [Online]. Available: [https://www.itu.int/en/ITU-T/focusgroups/net2030/Documents/White\\_Paper.pdf](https://www.itu.int/en/ITU-T/focusgroups/net2030/Documents/White_Paper.pdf)
- [2] M. Shafi *et al.*, "5G: A Tutorial Overview of Standards, Trials, Challenges, Deployment, and Practice," in *IEEE J. Sel. Areas in Commun.*, vol. 35, no. 6, pp. 1201-1221, Jun. 2017.
- [3] M. H. Alsharif, A. H. Kelechi, M. A. Albreem, S. A. Chaudhry, M. S. Zia, and S. Kim, "Sixth Generation (6G) Wireless Networks: Vision, Research Activities, Challenges and Potential Solutions." *Symmetry*, vol. 12, no. 4, p. 676, Apr. 2020.
- [4] M. Latva-aho and K. Leppänen, "Key drivers and research challenges for 6G ubiquitous wireless intelligence," University of Oulu, Sep. 2019. [Online]. Available: <http://jultika.oulu.fi/files/isbn9789526223544.pdf>
- [5] A. R. Mishra *et al.*, *Advanced Cellular Network Planning and Optimization*, U.K., Chichester: Wiley, 2007.
- [6] D. Tse and P. Viswanath, *Fundamentals of Wireless Communication*. New York, NY, USA: Cambridge Univ. Press, 2005.
- [7] H. Zhang, S. Chen, L. Feng, Y. Xie and L. Hanzo, "A universal approach to coverage probability and throughput analysis for cellular networks," *IEEE Trans. Veh. Technol.*, vol. 64, no. 9, pp. 4245-4256, Sep. 2015.
- [8] L. Yang, S. H. Song and K. B. Letaief, "Optimal overlay cognitive spectrum access with F-ALOHA in macro-femto heterogeneous networks," *IEEE Trans. Wireless Commun.*, vol. 15, no. 2, pp. 1323-1335, Feb. 2016.
- [9] J. G. Andrews, F. Baccelli and R. K. Ganti, "A tractable approach to coverage and rate in cellular networks," *IEEE Trans. Commun.*, vol. 59, no. 11, pp. 3122-3134, Nov. 2011.
- [10] S. Ahmadi, *LTE-Advanced: A Practical Systems Approach to Understanding 3GPP LTE Releases 10 and 11 Radio Access Technologies*, Academic Press, Nov. 2013.
- [11] M. K. Karakayali, G. J. Foschini, R. A. Valenzuela and R. D. Yates, "On the maximum common rate achievable in a coordinated network," in *Proc. IEEE Int. Conf. Commun.*, Jun. 2006, pp. 4333-4338.
- [12] G. Interdonato, E. Bjornson, H. Q. Ngo, and G. Larsson, "Ubiquitous cell-free Massive MIMO communications," *EURASIP J. Wireless Commun. Netw.*, vol. 2019, p. 197, Aug. 2019.
- [13] M. Matthaiou, O. Yurduseven, H. Q. Ngo, D. Morales-Jimenez, S. Cotton, and V. Fusco, "The road to 6G: Ten physical layer challenges for communications engineers," *IEEE Commun. Mag.*, vol. 59, no. 1, pp. 64-69, 2021.
- [14] H. Zhang, Y. Dong, J. Cheng, M. J. Hossain and V. C. M. Leung, "Fronthauling for 5G LTE-U ultra dense cloud small cell networks," *IEEE Wireless Commun.*, vol. 23, no. 6, pp. 48-53, Dec. 2016.
- [15] M. A. Habibi, M. Nasimi, B. Han and H. D. Schotten, "A comprehensive survey of RAN architectures toward 5G mobile communication system," *IEEE Access*, vol. 7, pp. 70371-70421, 2019.
- [16] C. Pan, M. ElKashlan, J. Wang, J. Yuan and L. Hanzo, "User-centric C-RAN architecture for ultra-dense 5G networks: challenges and methodologies," *IEEE Commun. Mag.*, vol. 56, no. 6, pp. 14-20, June 2018.
- [17] F. Tariq, M. R. A. Khandaker, K.-K. Wong, M. A. Imran, M. Bennis and M. Debbah, "A speculative study on 6G," *IEEE Wireless Commun.* vol. 27, no. 4, pp. 118-125, Aug. 2020.
- [18] H. Q. Ngo, A. Ashikhmin, H. Yang, E. G. Larsson and T. L. Marzetta, "Cell-free Massive MIMO versus small cells," *IEEE Trans. Wireless Commun.*, vol. 16, no. 3, pp. 1834-1850, Mar. 2017.
- [19] J. Zhang *et al.*, "PoC of SCMA-based uplink grant-free transmission in UCNC for 5G," *IEEE J. Sel. Areas Commun.*, vol. 35, no. 6, pp. 1353-1362, Jun. 2017.
- [20] G. Interdonato, P. Frenger and E. G. Larsson, "Scalability aspects of cell-free massive MIMO," in *Proc. IEEE Int. Conf. Commun.*, May 2019, pp. 1-6.
- [21] L. Dai and B. Bai, "Optimal decomposition for large-scale infrastructure-based wireless networks," *IEEE Trans. Wireless Commun.*, vol. 16, no. 8, pp. 4956-4969, Aug. 2017.
- [22] J. Wang, L. Dai, L. Yang, and B. Bai, "Clustered cell-free networking: a graph partitioning approach," submitted to *IEEE Trans. Wireless Commun.*, Mar. 2022, under review.
- [23] J. Wang, L. Dai, L. Yang, and B. Bai, "Rate-constrained network decomposition for clustered cell-free networking," accepted by *IEEE ICC*, 2022.
- [24] S. Buzzi and C. D'Andrea, "Cell-free massive MIMO: user-centric approach," *IEEE Wireless Commun. Lett.*, vol. 6, no. 6, pp. 706-709, Dec. 2017.

- [25] Y. Zhang and L. Dai, "On the optimal placement of base station antennas for distributed antenna systems," *IEEE Commun. Lett.*, vol. 24, no. 12, pp. 2878-2882, Dec. 2020.
- [26] X. Yu, C. Li, J. Zhang, M. Haenggi and K. B. Letaief, "A unified framework for the tractable analysis of multi-antenna wireless networks," *IEEE Trans. Wireless Commun.*, vol. 17, no. 12, pp. 7965-7980, Dec. 2018.
- [27] M. Bashar, K. Cumanan, A. G. Burr, M. Debbah and H. Q. Ngo, "On the uplink max-min SINR of cell-free massive MIMO systems," *IEEE Trans. Wireless Commun.*, vol. 18, no. 4, pp. 2021-2036, Apr. 2019.
- [28] G. Interdonato, H. Q. Ngo, E. G. Larsson and P. Frenger, "How much do downlink pilots improve cell-free massive MIMO?" in *Proc. IEEE GLOBECOM*, 2016, pp. 1-7.
- [29] S. Buzzi, C. D'Andrea, A. Zappone and C. D'Elia, "User-centric 5G cellular networks: Resource allocation and comparison with the cell-free massive MIMO approach," in *IEEE Trans. Wireless Commun.*, vol. 19, no. 2, pp. 1250-1264, Feb. 2020.
- [30] C. E. Shannon, "A mathematical theory of communication," *The Bell Syst. Tech. J.*, vol. 27, no. 3, pp. 379-423, Jul. 1948.
- [31] Z. M. Balogh, O. O. Ibrogimov, B.S. Mityagin, "Functional equations and the Cauchy mean value theorem," *Aequat. Math.*, vol. 90, pp. 683-697, 2016.
- [32] Q. Du, V. Faber, and M. Gunzburger, "Centroidal voronoi tessellations: Applications and algorithms," *SIAM Rev.* vol. 41, no. 4, pp. 637-676, 1999.



**Lu Yang** (S'13-M'20) received the B.E. degree (first class Hons.) in Information Engineering from Xi'an Jiaotong University (XJTU) in 2011, and the Ph.D. degree from the Department of Electronic and Computer Engineering, Hong Kong University of Science and Technology (HKUST) in 2016. From 2016 to 2019, she was a Senior Engineer with the Hong Kong Applied Science and Technology Research Institute (ASTRI), where she served as a principal technical consultant commissioned by the Hong Kong Office of the Communications Authority (OFCA) on Hong Kong's 5G spectrum allocation. She is currently a Researcher with Theory Lab, 1212 Labs, Huawei Technologies Co., Ltd. She was an awardee of Hong Kong PhD Fellowship (HKPF) 2011, and a recipient of Top 50 Papers Award in IEEE Globecom 2014. Her broad research interests include wireless communications, 5G/B5G/6G networking, information theory, stochastic geometry, and random matrix theory.



**Ping Li** received her Ph.D. in mathematics from Shandong University, China. In 2020, she joined Huawei Technologies Co., Ltd. where she is currently a Senior Theory Researcher with the Theory Lab. Her current research interest include graph theory, matroid theory and information theory.



**Miaomiao Dong** received the B.Eng. degree from Northwestern Polytechnical University, in 2010, the M.Eng. degree from Xidian University, in 2013, and the Ph.D. from City University of Hong Kong, in 2020. Since 2020, he has been a researcher in the Theory Lab, Central Research Institute, 1212 Labs, Huawei Technologies Co., Ltd. His current research interests include intelligent reconfigurable surface communications, Massive MIMO precoder design, and wireless localizations.



**Bo Bai** (S'09-M'11-SM'17) received the B.S. degree with the highest honor in School of Communication Engineering from Xidian University, Xi'an China, 2004, and the Ph.D. degree in Department of Electronic Engineering from Tsinghua University, Beijing China, 2010. He received the Honor of Outstanding Graduates of Shaanxi Province and the Honor of Young Academic Talent of Electronic Engineering in Tsinghua University. He was a Research Assistant from April 2009 to September 2010 and a Research Associate from October 2010 to April 2012 with the Department of Electronic and Computer Engineering, Hong Kong University of Science and Technology. From July 2012 to January 2017, he was an Assistant Professor with the Department of Electronic Engineering, Tsinghua University. He has obtained the support from Backbone Talents Supporting Project of Tsinghua University. Currently, he is an Information Theory Scientist and Director of Theory Lab, 1212 Labs, Huawei Technologies Co., Ltd., Hong Kong. He's research interests include semantic information theory, B5G/6G networking, and graph informatics.

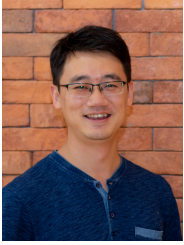
He is an IEEE Senior Member, and has authored more than 130 papers in major IEEE and ACM journals and conferences, 2 book chapters, and 1 textbook. He is one of the founded vice chairs of IEEE TCCN SIG on Social Behavior Driven Cognitive Radio Networks. He served as a committee member in IEEE ComSoc WTC and IEEE ComSoc SPCE. He served as a TPC co-chair of IEEE Infocom 2018 - 1st AoI Workshop and IEEE Infocom 2019 - 2nd AoI Workshop, a TPC co-chair of IEEE ICC 2018, and an Industrial Forum & Exhibition co-chair of IEEE HotICN 2018. He also served as a TPC member for several IEEE conferences such as ICC, Globecom, WCNC, VTC, and ICC. He served as a reviewer for several major IEEE and ACM journals and conferences. He was the recipient of the Student Travel Grant at IEEE Globecom 2009. He was invited as a Young Scientist Speaker at IEEE TTM 2011. He was a recipient of the Best Paper Award in IEEE ICC 2016.



**Dmitry Zaporozhets** received the specialist degree form Saint-Petersburg State University in 2001, and the Ph.D. and Sc.D. degrees form the St. Petersburg Department of Steklov Mathematical Institute in 2005 and 2017, where he is currently a Deputy Director for Science and the Head of the Laboratory of Statistical Methods. He is a Professor of the Russian Academy of Sciences, a member of the Saint-Petersburg Mathematical Society and the European Mathematical Society, an Associate Editor of "Stochastic Processes and their Applications" Journal. He was the recipient of the Gold medal in the International Mathematical Olympiad held in Toronto in 1995 and the Prize of the Government of Saint-Petersburg for outstanding scientific achievements in the field of science and technology in 2014. His main areas of research are theory of probability, stochastic geometry, convex geometry, and geometry of numbers.



**Xiang Chen** received the B.E. degree in Electronics and Information Engineering from the Huazhong University of Science and Technology (HUST) in 2008, and the Ph.D. degree from the Department of Electronic and Computer Engineering, Hong Kong University of Science and Technology (HKUST), in 2013. After graduation, he was a Senior Engineer with the Hong Kong Applied Science and Technology Research Institute (ASTRI) from 2013 to 2019. He is currently a Principal Engineer with the Theory Lab, Central Research Institute, 1212 Labs, Huawei Technologies Co., Ltd. His broad research interests include system and algorithm design for emerging wireless technologies and theory, including massive MIMO, interfering networks, and B5G/6G cell-free architecture.



**Wei Han** (S'12-M'19) received the B.S. degree from Tsinghua University in 2011 and the Ph.D. degree from The Hong Kong University of Science and Technology (HKUST) in 2018. He is currently a Senior Researcher with the Theory Lab, Central Research Institute, 2012 Labs, Huawei Tech. Investment Co., Ltd. His research interests include wireless communications, and information theory.



**Baochun Li** received his Ph.D. degree from the Department of Computer Science, University of Illinois at Urbana-Champaign, Urbana, in 2000. Since then, he has been with the Department of Electrical and Computer Engineering at the University of Toronto, where he is currently a Professor. He holds the Bell Canada Endowed Chair in Computer Engineering since August 2005. His research interests include large-scale distributed systems, machine learning, security, cloud computing, and wireless networks. He is a member of the ACM and a fellow of the

IEEE.